Tellus SERIES B CHEMICAL AND PHYSICAL METEOROLOGY
PUBLISHED BY THE INTERNATIONAL METEOROLOGICAL INSTITUTE IN STOCKHOLM

New particle formation in the presence of a strong biomass burning episode at a downwind rural site in PRD, China

By Z. B. WANG[1], M. HU[1]*, D. L. YUE[1], L. Y. HE[2], X. F. HUANG[2], Q. YANG[1], J. ZHENG[3], R. Y. ZHANG[1,3] and Y. H. ZHANG[1], *[1]State Key Joint Laboratory of Environmental Simulation and Pollution Control, College of Environmental Sciences and Engineering, Peking University, Beijing 100871, China; [2]Key Laboratory for Urban Habitat Environmental Science and Technology, School of Environment and Energy, Peking University Shenzhen Graduate School, Shenzhen 518055, China; [3]Department of Atmospheric Science, Texas A&M University, College Station, Texas 77843, USA*

(Manuscript received 25 October 2012; in final form 22 January 2013)

ABSTRACT

In order to characterise the features of particle pollution in the Pearl River Delta (PRD) region, a 1-month intensive campaign was conducted at the rural supersite (Kaiping) in the autumn of 2008. In total, 12 new particle formation (NPF) events are identified out of 30 campaign days. The results show that in the case of higher source and sink values, the result of the competition between source and sink is more likely the key limiting factor to determine the observation of NPF events at Kaiping. One episode with consecutive NPF events in the presence of strong biomass burning plume was observed between 10 and 15 November. The elevation of particle volume concentration (6.1 $\mu m^3/cm^3$/day) is due to the coaction by the local biomass burning and secondary transformation. Organics and sulphates are the major components in PM_1, accounting for 42 and 35% of the mass concentration, respectively. In this study, a rough estimation is applied to quantify the contributions of diverse sources to the particle number concentration. On average, the primary emission and secondary formation provide 28 and 72% of particle number concentration and 21 and 79% of mass concentration, respectively.

Keywords: new particle formation, sulphuric acid, condensation sink, biomass burning, secondary formation

1. Introduction

Particulate matter (PM), especially fine particles, is of interest because of its effects on human health and climate change (Poschl, 2005). The smaller the particles, with higher number concentration and surface area per unit mass, the more easily absorbed are the toxic air pollutants (Sioutas et al., 2005). Moreover, ambient particles directly affect the global climate system by scattering and absorption of solar radiation (Stier et al., 2007), and by indirectly acting as cloud condensation nuclei (CCN) and ice nuclei (IN) (Lohmann and Feichter, 2005). However, all these effects depend both on the particle size distribution and chemical composition, which can not only affect the lifetime and optical properties but also provide information on the source and transformation mechanisms in the atmosphere (Kannosto et al., 2008).

The Pearl River Delta (PRD) area is one of the biggest city clusters in China. The rapid economic development and urbanisation are accompanied by serious air pollution problems, from an urban to a regional scale. Several field campaigns were conducted in the last decade, and the results indicated the feature of complex air pollution, of which fine particles and ozone are the major focus. The annual average $PM_{2.5}$ mass concentration was 71 $\mu g/m^3$ during 2002–2003 at urban Guangzhou (Hagler et al., 2006), which is double that of the new China National Air Quality Standards of a $PM_{2.5}$ annual average of 35 $\mu g/m^3$. The average PM_1 concentrations were 31 and 33 $\mu g/m^3$ at the two downwind rural sites, Back Garden (2006) and Kaiping (2008), respectively, in which the dominant components were organic matters and sulphates (Huang et al., 2011; Xiao et al., 2011).

*Corresponding author.
e-mail: minhu@pku.edu.cn

Citation: Tellus B 2013, **65**, 19965, http://dx.doi.org/10.3402/tellusb.v65i0.19965

This implied that the submicron particles were mainly formed through the secondary transformation process. In addition, the local biomass burning also contributed to the decline in the air quality in the PRD region (Andreae et al., 2008; Huang et al., 2010; Yuan et al., 2010). However, most of these studies mainly focused on the particle mass concentration and chemical composition in fine particles. Only a few research findings on the particle number size distribution and new particle formation (NPF) have been reported (Liu et al., 2008; Gong et al., 2010; Yue et al., 2010).

To get a better understanding on the properties of fine particle pollution in the PRD, aerosol physical and chemical parameters were measured during the intensive campaign in autumn 2008. One episode with continuous nucleation events in the presence of intensive biomass burning is discussed in this investigation. The variations of primary and secondary pollutants are quantified, and the contribution of the local biomass burning to the particle number concentration is estimated.

2. Experimental methods

2.1. Site description

The parallel intensive field observations were conducted from 10 October to 18 November in 2008 at two sites: an urban site in Guangzhou city (23.13°N, 113.26°E) and a rural site at Kaiping (22.32°N, 112.53°E) which is 120 km away from Guangzhou to the southwest. Under the influence of the Asian monsoon, the dominant air mass comes to PRD from the northeast in fall. Hence, the Kaiping site could be assumed to be a downwind receptor site. Most of the high time-resolution on-line instruments were placed on the third floor of the building at the Kaiping supersite (about 10 m above the ground level), which is surrounded by shrubs and eucalyptus forest. A detailed geographic description of the measurement site is presented in Huang et al. (2011).

2.2. Instrumentation

A Scanning Mobility Particle Sizer (SMPS; TSI model 3936) system was used to measure the dry particle number size distribution in the size range 15–700 nm (mobility diameter). The whole system contains one Differential Mobility Analyser (DMA; TSI model 3085) and one Condensation Particle Counter (CPC; TSI model 3772). The flow rate was 0.3 L/min for the sample air and 3.0 L/min for the sheath air. Flow rate was checked once a day with a bubble flow meter. The relative humidity in the whole system was kept below 40%. The size-dependent diffusion losses in connecting tubes were calculated as described in a previous publication (Lin et al., 2007). The time resolution was 5 min per scan for the system.

The gaseous sulphuric acid concentration was measured using an Atmospheric Pressure Ion Drift-Chemical Ionisation Mass Spectrometry (AP-ID-CIMS), which was developed by Texas A & M University (TAMU). The original time resolution was 12 s, and the data were averaged to 5 min to reduce statistical error and to be consistent with the particle number size distribution. Detailed information of the instrument and measurement was introduced by Zheng et al. (2011).

The chemical components in fine particles were carried out using an Aerodyne High-Resolution Time-of-Flight Aerosol Mass Spectrometer (HR-ToFAMS) at the Kaiping site. Detailed instrumental and parameter descriptions of HR-ToFAMS can be found in Huang et al. (2011). The black carbon (BC) was measured by a Multi-Angle Absorption Photometer (MAAP; Thermo Model 5012). Both HR-TofAMS and MAAP results were used to make up mass concentration of PM_1.

3. Results and discussion

3.1. General overview

Figure 1a exhibits the temporal variations of particle number size distributions during the whole measurement periods. The measured ambient particle number size distributions are fitted and parameterised by a multiple log-normal distribution function (Seinfeld and Pandis, 1998):

$$\frac{dN}{d\log Dp} = \frac{N_i}{\sqrt{2\pi}\log\sigma}\exp\left[-\frac{\left(\log Dp - \log\overline{Dp_i}\right)^2}{2(\log\sigma)^2}\right] \quad (1)$$

Here N_i and $\overline{Dp_i}$ are the total number concentration and geometric mean diameter (GMD) of mode i, respectively, while σ is the geometric mean standard deviation of the distribution. Three modes are identified corresponding to the nucleation mode (15–25 nm), Aitken mode (25–100 nm) and accumulation mode (100–700 nm). On average, GMD of the three modes are 20 nm, 78 nm and 211 nm during the whole campaign period. The higher GMD in each mode is observed at Kaiping rural site compared with the previous study in Guangzhou (Yue et al., 2010), which might relate to the ageing process during the transport. During the measurement period, the total particle number concentration (15–700 nm) was $11\,000 \pm 6500$ cm^{-3}, which was lower than the observations in the size range 20 nm–10 μm at Guangzhou ($29\,000 \pm 11\,000$ cm^{-3}) and Backgarden ($17\,000 \pm 8\,000$ cm^{-3}) in 2006 (Yue et al., 2010). The mean particle number concentrations in the three modes are 1000 ± 2100 cm^{-3}, 5800 ± 4700 cm^{-3}, 4200 ± 2400 cm^{-3}.

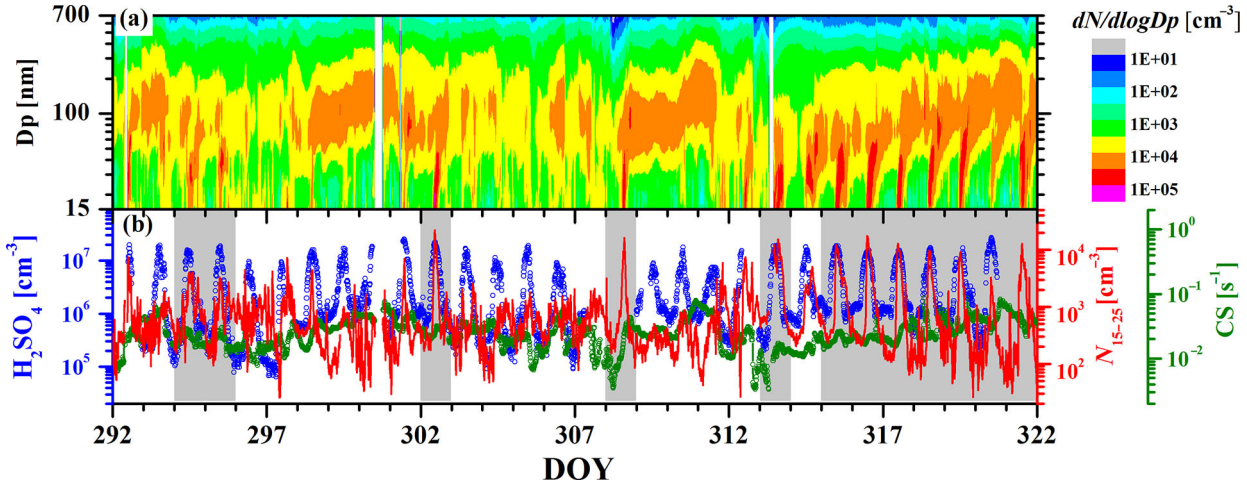

Fig. 1. Time series for (a) particle number size distributions and (b) sulphuric acid (H_2SO_4, blue empty dot), condensation sink (*CS*, green line with empty dot) and 15–25 nm particle number concentrations ($N_{15–25}$, red line) for the measurement period. The new particle formation event days are presented on a grey background. The x-axis is presented by DOY (day of year), 1 January is defined as day 1.

The number concentration of Aitken mode particles is lower than the study in Beijing, 15 900 cm^{-3} (Wu et al., 2008), and Shanghai, 8200 cm^{-3} (Du et al., 2012), which may be due to the influence of intensive local traffic emissions in urban environments.

The criterion for discerning NPF events is the bursting of the nucleation mode particle concentration (Birmili and Wiedensohler, 2000). In total, 12 NPF events are identified out of 30 measurement days from 18 October (day 292) to 16 November (day 321). The frequency of the NPF event is 40%, which is higher than that in our previous study (26%) at a rural site Xinken of the PRD (Liu et al., 2008). It is evidenced that both the $N_{15–25}$ and H_2SO_4 concentrations have strong diurnal variations on NPF days (grey background, see Fig. 1b). The nucleation mode particles are formed clearly around 10:00 AM, followed by subsequent growth until midnight.

Table 1 lists the various parameters on NPF event days and non-event days before the nucleation events start (9:00–12:00 AM). The mean temperature (T) and relative humidity (RH) are 23°C and 55%, respectively, on NPF event days, which are lower than that on non-event days (27°C and 67%). This result is consistent with the theory that lower RH is favourable to the enhancement of atmospheric nucleation (Hamed et al., 2011). In addition, the mean wind speed (WS) is 2.7 m s^{-1} on NPF event days, about 1.4 times higher than that on non-event days (1.9 m s^{-1}), which is favourable to the dilution of the pollutants.

The mean sulphuric acid concentration (during 9:00–12:00 AM) is 1.3×10^7 cm^{-3}, which is higher than that on non-event days (0.9×10^7 cm^{-3}). The condensation sink (CS) describes how rapidly vapour molecules condense onto the particles, which could be used to represent pre-existing particle concentration (Kulmala et al., 2001). Its value could be calculated using eq. (2):

$$CS = 2\pi D \sum \beta DpN \quad (2)$$

where D is the diffusion coefficient of the condensing vapour, β is the transitional regime correction factor, Dp is the aerosol particle diameter and N is its number concentration. However, it should be noted that in this study, the CS values are achieved based on the dry particle number size distributions, which may underestimate the real CS values in ambient humidity (Kulmala et al., 2001). The mean CS on NPF event days (0.025 s^{-1}) is typically lower than that on non-event days (0.030 s^{-1}). The CS value on NPF event days is 5–10 times higher than other observations at rural sites (see Table 2), even the urban environments like Marseille (0.003–0.015 s^{-1}) and Athens (0.006–0.013 s^{-1}), but lower than that in the

Table 1. Comparisons of various parameters between NPF event days and non-event days (during 9:00–12:00)

	No.	T (°C)	RH (%)	WS (m s^{-1})	H_2SO_4 (10^7 cm^{-3})	CS (10^{-2} s^{-1})	H_2SO_4/CS (10^8 cm^{-3}·s)
NPF event	13	23 ± 3.9	55 ± 12	2.7 ± 1.4	1.3 ± 0.4	2.5 ± 1.1	6.2 ± 2.7
Non-event	17	27 ± 3.0	67 ± 8.3	1.9 ± 1.4	0.9 ± 0.5	3.0 ± 1.2	3.7 ± 2.4

Table 2. Comparisons of the condensation sink values with other studies at rural sites on NPF event days

Site	Sampling period	No. of events	CS ($\times 10^{-2}$ s^{-1})	Ref.
Kaiping	Oct. 18–Nov. 16, 2008	12	0.3–8.6	This study
Hyytiälä	Winters 1997–2001	34	0.02–0.7	Kulmala et al. (2005)
Po Valley	2002–2005	136	0.9–1.96	Hamed et al. (2007)
K-puszta	May 22–June 29, 2006	26	0.06–1.4	Yli-Juuti et al. (2009)
Melpitz	July, 2003–June, 2005	158	0.7 (mean)	Jaatinen et al. (2009)
Botsalano	July 20, 2006–Feb. 5, 2008	988	0.4 (mean)	Vakkari et al. (2011)

polluted regions such as New Delhi, 0.005–0.007 s^{-1} (Kulmala et al., 2005).

The mean SO_2 concentration is 8.6 ± 8.3 ppb during the whole campaign period, which is 3–10 times higher than the observations in Europe and America (Mikkonen et al., 2011), indicating that more sulphuric acid should be produced. However, the median value of ambient sulphuric acid concentration is 1.3×10^6 cm^{-3}, which is comparable with other field observations. The explanation for this fact is the higher CS at the Kaiping site. The higher number concentration of newly formed particles is observed when the ratio of sulphuric acid concentration to CS is larger, as shown in Fig. 2. The mean ratios before the nucleation events start are 6.2 and 3.7 cm^{-3}·s on NPF event days and non-event days, respectively. The NPF event is the product of the competition between source and sink (here expressed as sulphuric acid concentration and CS). Hence, in the case

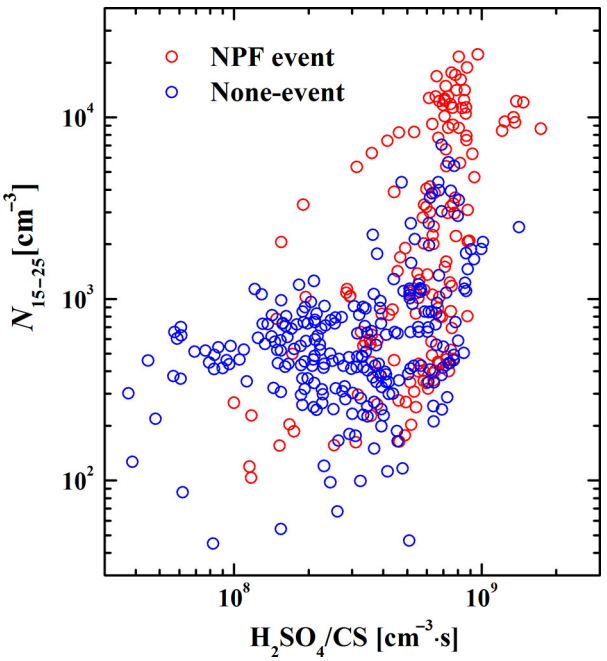

Fig. 2. The relationship between the number concentration of 15–25 nm particles and the ratio of sulphuric acid concentration to condensation sink. The data are from 09:00 to 12:00. NPF event days (red), Non-event days (blue).

of higher primary emission (SO_2), the result of the competition between source and sink is more likely the key limiting factor to determine the observation of NPF events in Kaiping, which is consistent with the study in the polluted urban environment of Beijing (Wang et al., 2011). In addition, we should notice that during the continuous NPF events episode (10–16 November), the maximum H_2SO_4 concentration is observed on 15 November, with the peak value of 2.7×10^7 cm^{-3}. On the contrary, the lower strength of NPF occurred with the maximum N_{15-25} value of 3300 cm^{-3}. This is because the mean CS (during 9:00–12:00) is 0.036 s^{-1} on 15 November which is higher than that (0.025 s^{-1}) on the previous 5 d, implying that the strength of NPF event is controlled by the pre-existing particles in the rural site of Kaiping.

The nearly linear increase in the particle mean diameter is observed, and the growth rates vary from 3.2 nm/h to 13.5 nm/h for 12 NPF events, which is in the typical range (1–20 nm/h) as summarised by the review article (Kulmala et al., 2004). The mean growth rate is 7.4 nm/h, which is slightly higher than that in Mexico City, 0.5–9 nm/h (Dunn et al., 2004), and lower than that in New Delhi, 11.6–18.1 nm/h (Monkkonen et al., 2005). The newly formed particles would be scavenged by coagulation onto the pre-existing particles before reaching the detectable size range, so they have to grow faster especially in a polluted area. Therefore, the higher grow rate is expected at the Kaiping site. In addition, it is worth noting that the increase of N_{15-25} is preceded by an increase in sulphuric acid concentration. The average time delay, indicating the time it takes for the clusters to grow from the nucleation size (~ 1.5 nm) to the detectable size (15 nm in this study), is approximately 1.6 ± 0.5 h over all the 12 NPF events. This time delay is also found in other studies (Sihto et al., 2006; Riipinen et al., 2007; Kuang et al., 2008).

3.2. *NPF in the biomass burning plume episode*

The characteristics of submicron aerosols and volatile organic compounds (VOCs) in the same campaign have been analysed and reported previously (Yuan et al., 2010; Huang et al., 2011). HR-ToFAMS results show that the measured PM_1 concentration is 33 ± 18 μg/m^3 during

the campaign period. Organic matter and sulphates are the major components in submicron aerosols, accounting for 33.8 and 33.7%, respectively. In addition, three kinds of organic components, including one biomass burning (BBOA) and two oxygenated organic aerosols (SV-OOA and LV-OOA), had been identified using the Positive Matrix Factorisation (PMF) model, which on average accounts for 24, 40 and 36% of the total organic mass, respectively. High BBOA concentration (9.1 $\mu g/m^3$) was observed after 12 November, indicating the intensive biomass burning. Moreover, the results obtained from the Proton Transfer Reaction-Mass Spectrometer (PTR-MS) reveal that biomass burning contributes 19.6–34.4% of the VOCs mixing ratios during 12–18 November, while only 6.2–12.6% from 19 October to 11 November (Yuan et al., 2010). This is typical of the PRD region at the start of November, as the local farmers burn the rice straws in the fields after harvest.

Even during the intensive biomass burning plume, consecutive NPF events are observed from 10 to 15 November at Kaiping site (see Fig. 3a). Figure 3b and 3c exhibit the temporal evolutions of meteorological parameters. The T and RH show the increasing trend during the episode. On average, the T and RH are 18°C and 47% on 10 November, corresponding to 22°C and 70% on 15 November, respectively. Meanwhile, the significant diurnal pattern of wind direction is observed, with the wind mainly coming from the northeast with higher speed in the daytime and becoming calm at night. At the beginning of the episode, the wind speed is up to 5 m s^{-1} on average in the early hours of 10 November, causing the dilution of the pollutants, while the PM_1 concentration is lower than 20 $\mu g/m^3$ (Fig. 3d). The more stable meteorological condition with low wind speed, high T and RH is formed gradually during the episode. These hot and humid conditions are ideal for pollution build-up.

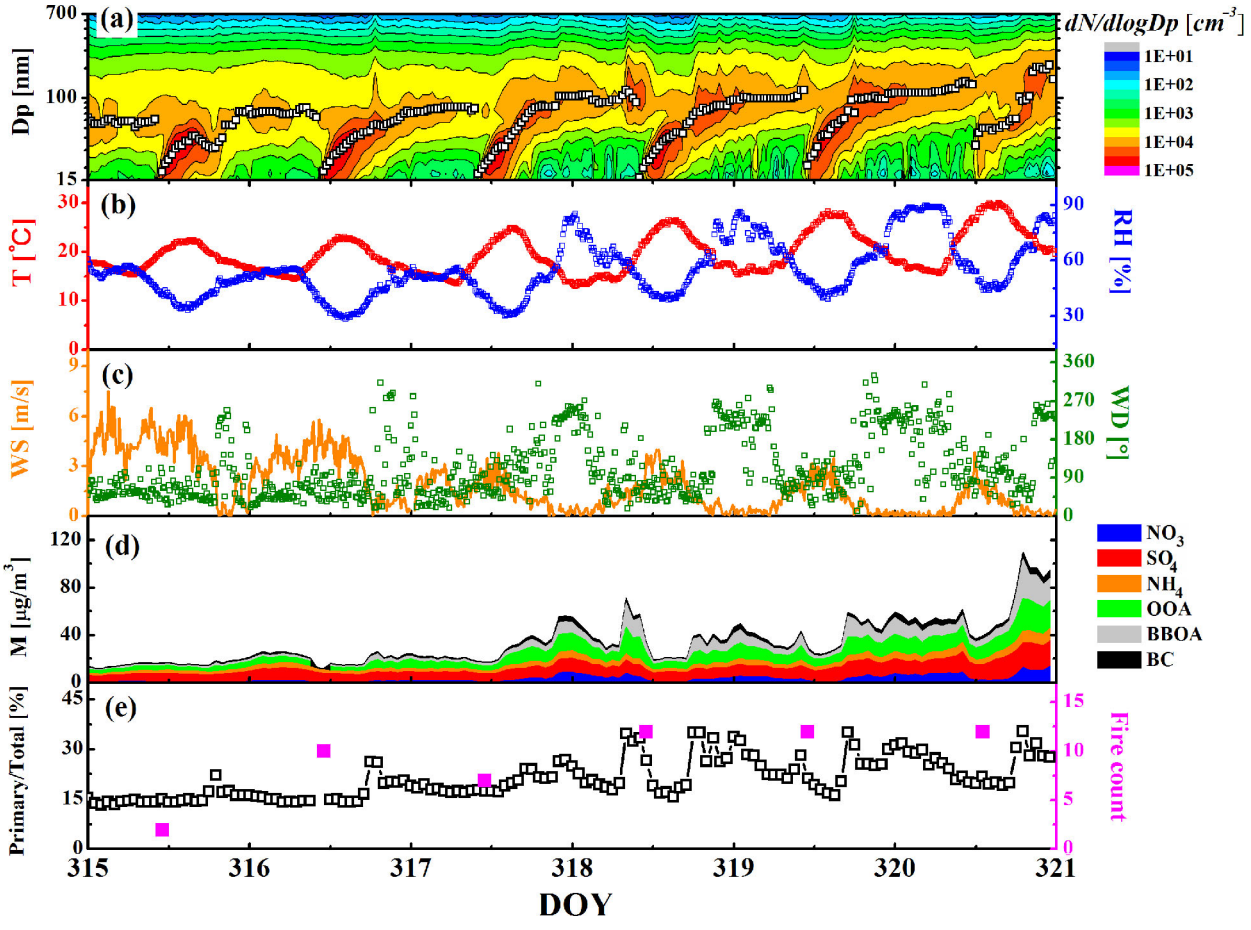

Fig. 3. Time series of (a) particle number size distribution and the mean diameter of the dominating mode; (b) Temperature (T, red) and Relative Humidity (RH, blue); (c) Wind Speed (WS, orange) and Wind Direction (WD, green); (d) PM_1 species concentrations; and (e) the ratio of primary emission to total mass concentration and fire count (pink) in PRD region during the episode.

The regional transport from the central PRD areas is the major origin of the pollutants at the downwind rural site of Kaiping (Huang et al., 2011). In addition, the local biomass burning is another reason that leads to the air pollution, as described above. As a result, the PM_1 concentration reached 104 μg/m^3 in the evening of 15 November, which was five times higher compared with the beginning of the episode. On average, organics and sulphates are the major contributors to PM_1 mass concentration, accounting for 42 and 32% during the episode, respectively. In this investigation, we classify sulphate, nitrate, ammonium and OOA (sum of LV-OOA and SV-OOA) as secondary components, while BBOA and BC are regarded as primary components. It should be noted that the BC concentration in PM_1 is overestimated because it is measured for $PM_{2.5}$ by MAAP in this campaign. The time evolutions of diverse components are displayed in Fig. 3d. The contributions of primary and secondary components are 21 and 79% on average, respectively. The mean hourly mass concentration of secondary components was over 70 μg/m^3 on the night of 15 November compared with about 12 μg/m^3 at the beginning of the episode. However, the relative mass fraction of secondary components did not elevate due to the influence of the intensive local biomass burning (see Fig. 3e). The mass concentrations of primary components showed frequent irregular peaks, corresponding to the abrupt variations of the GMD in the dominating mode (mainly in the size range of 60–110 nm). The minimum and maximum concentrations are 1.6 μg/m^3 and 39 μg/m^3, respectively. The contribution of primary components to PM_1 could be up to 37% during the episode. The number of daily fire hotspots detected by the Moderate Resolution Imaging Spectroradiometer (MODIS) instruments aboard the Terra and Aqua satellites (http://modis.gsfc.nasa.gov/) in the whole PRD region is presented in Fig. 3e. The appearance time of biomass burning sources and the peaks of primary components are not totally consistent. The cause of this phenomenon is limited by the MODIS resolution, not all the local combustion sources are counted. However, the smell of burning could be easily detected during the episode.

The peak diameter of particle number size distribution is shifted from 40 nm to 140 nm resulting in the accumulation of pollutants (see Fig. 4a). Particle number concentrations are dominated by the Aitken mode particles, which accounted for 66% of the total number of concentrations on 10 November, contrasting with the 60% contributed by accumulation mode particles on 15 November. As a result, the particle volume concentration presents the sustained increase (about 6.1 μm^3/cm^3/day, if the aerosol density is assumed as 1.7 g/cm^3, then the mass concentration build-up is about 10 μg/m^3/day) during the episode.

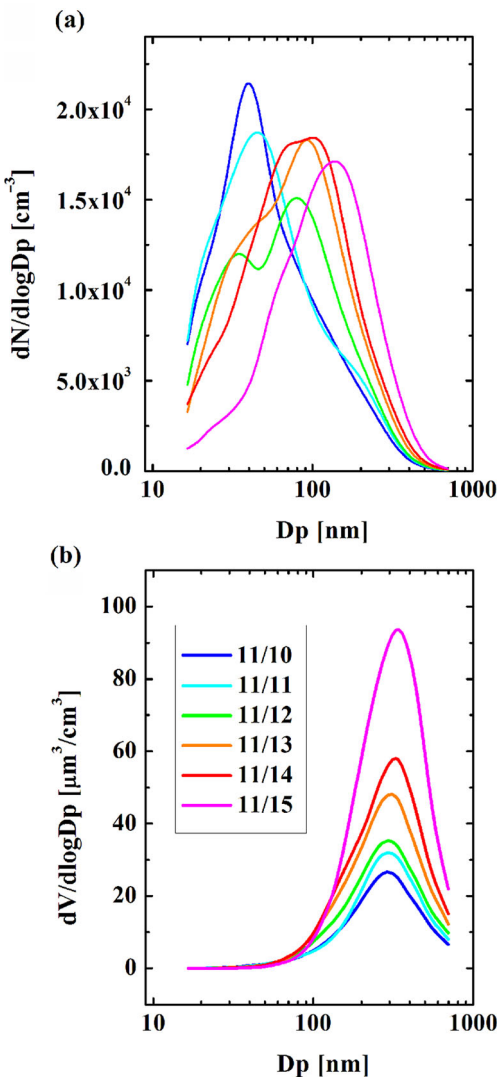

Fig. 4. Time evolutions of (a) particle number size distributions and (b) particle volume size distributions during the episode. Different colour lines represent the mean distribution.

3.3. Quantitative analysis of the primary and secondary sources of particle number concentrations

Figure 5a describes that various components exhibit different trends as the PM_1 mass concentration increased. The relative mass fraction of OOA is steady, in the range of 25–28%. Conversely, the contributions of primary species show the significant elevation from 16% at 10–20 μg/m^3 to 30% at over 60 μg/m^3. The entire increasing percentage is mainly contributed by BBOA. The same enhancement of nitrate as BBOA is also observed which might be influenced by the combustion process. All these results suggest that the important contribution of local emission to mass concentration of submicron particles. The variations of particle number concentrations in various modes with mass

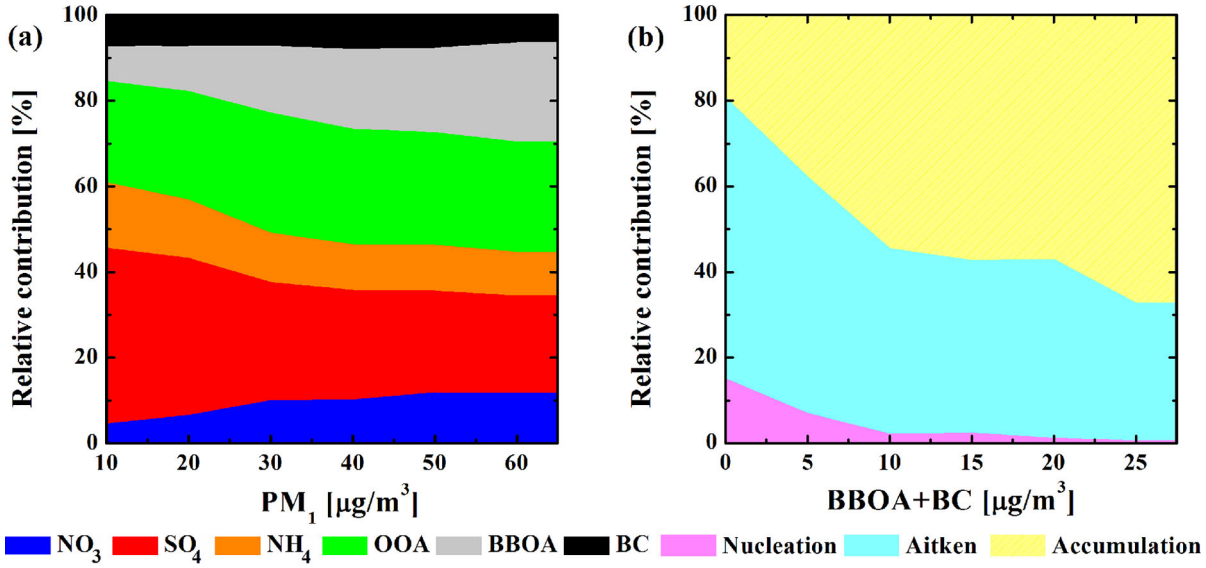

Fig. 5. The variations of (a) the relative contribution of different components, with PM_1 mass concentration; (b) the relative contribution of particle number concentration in different modes, with primary species (BBOA and BC) mass concentration.

concentrations of primary components are shown in Fig. 5b. It is significant that the relative number concentration fraction of accumulation mode particles shows the same trend as the mass concentration of primary species. The contribution is more than 50% at over 10 μg/m^3 and close to 70% when the mass concentration caused by local emission is more than 25 μg/m^3. Although the accumulation mode particles may not have all formed during the combustion process, it should not be ignored when we discuss the source of the particles.

A rough method to quantify the contributions of various sources to the particle number concentrations is applied in this research. This method is used in other research to distinguish the contributions of primary emissions and NPF enhancements by vehicle exhaust emissions in urban ambient air (Rodriguez and Cuevas, 2007). The influence of traffic emissions is not observed at the Kaiping rural site; however, it is replaced by the local biomass burning. Both BC and BBOA are assumed to be the markers for primary emissions, as described above. Hence, the ambient particle number concentration is split into two components: emitted by local emissions and formed by nucleation, which is considered an important formation mechanism of secondary particles via gas-to-particles transformation. However, it is also worth pointing out that the technique used in this study is suitable for sites only affected by the biomass burning. This is due to the fact that if the site is affected by other primary sources, such as traffic emissions, it is hard to distinguish the influences of traffic emission and biomass burning because they have the same indicator (BC). In addition, the biomass burning should not be far away from the sampling site. This is because the number of concentrations tends to drop under the effects of coagulation during transportation (Rose et al., 2006), resulting in a decrease in the S_1 slope (highlighted in Fig. 6).

Figure 6 displays the scatter plots of the total number concentration (N) versus the mass concentration of primary species (Pri.) during the whole episode. The data-set was mostly comprised between two well-defined slopes, S_1 and S_2, representing the minimum and maximum N/Pri. ratio, 0.44×10^3 particles/μg Pri. and 14.1×10^3 particles/μg Pri., respectively. The statistical analysis of the N/Pri. ratio shows that slope S_1 is very close to the 1st percentile (0.49×10^3 particles/μg Pri.), whereas S_2 approaches the 99th percentile (12.5×10^3 particles/μg Pri.).

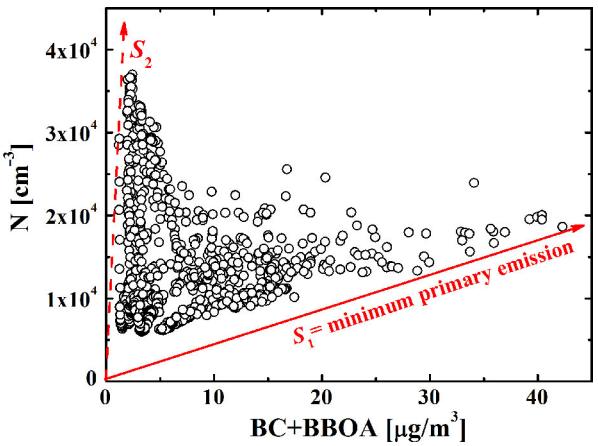

Fig. 6. Scatter plot of the total particle number concentration (N) versus the primary emissions (BBOA + BC). S_1 and S_2 indicate the lines of the minimum and maximum slopes which comprise the N-vs.-Pri. data, respectively.

To evaluate and quantify the contributions of the different sources leading to the particle number concentration, the total particle number concentration is segregated into two components:

$$\mathrm{N1} = S_1 \times \mathrm{Pri.} \quad (3)$$

$$\mathrm{N2} = \mathrm{N} - \mathrm{N1} \quad (4)$$

where $S_1 = 0.44 \times 10^3$ particles/μg Pri. is the minimum slope shown in Fig. 6. N1 represents the number concentration of particles formed by local biomass burning. N2 accounts for the particles formed by secondary transformation.

The minimum N-vs.-Pri. slope is used to calculate the number concentration contributed by biomass burning. Hence its contribution is underestimated. On average, N1 and N2 provide 28±21% and 72±21% to the total particle number concentration, respectively. The relatively larger standard deviation of primary particles might be due to the large uncertainty about local emissions. N1 shows the increasing trend and correlates well with particle surface area concentration (see Fig. 7a), especially at the random peaks during the episode. This phenomenon is good evidence to prove the reasonable of this quantitative method. Other studies show particle number size distribution of combustion source with a peak between 0.12 and 0.32 μm (located in the accumulation mode) which is the major contributor to the surface area concentration (Li et al., 2007). Figure 7b displays the time revolutions of N2 and sulphuric acid concentration. The similar diurnal variation between N2 and sulphuric acid concentration is observed on NPF event days.

4. Conclusions

The characters of submicron particles in the PRD region are investigated based on a 1-month (18 October–16 November) intensive campaign conducted at a downwind rural site. In total, 12 NPF events are identified during 30 d and the frequency of the NPF event is 40%. Gaseous sulphuric acid shows the similar diurnal variation with the number concentration of nucleation mode particles (15–25 nm). The CS values (during 9:00–11:00) were 0.025 s^{-1} and 0.030 s^{-1} on NPF event and non-event days, respectively, which are higher than the observations in Europe. The higher number concentration of newly formed particles is observed when the ratio of sulphuric acid concentration to CS value is larger. The mean ratios before the nucleation event start are 6.2 and 3.7 cm^{-3} on NPF event days and non-event days, respectively, indicating that the result of the competition between source and sink is more likely the key limiting factor to determine the observation of NPF events in Kaiping. The particle growth rates vary from 3.2 nm/h to 13.5 nm/h, with a mean value of 7.4 nm/h for 12 NPF event days.

One episode, including consecutive nucleation event days in the presence of strong biomass burning plume, is observed from 10 to 15 November. Under the control of stagnant meteorological conditions (high T and RH, low WS), the mass concentration of fine particles elevates from 12 $\mu g/m^3$ to 104 $\mu g/m^3$ during the episode which could be attributed to the local biomass burning and secondary transformation.

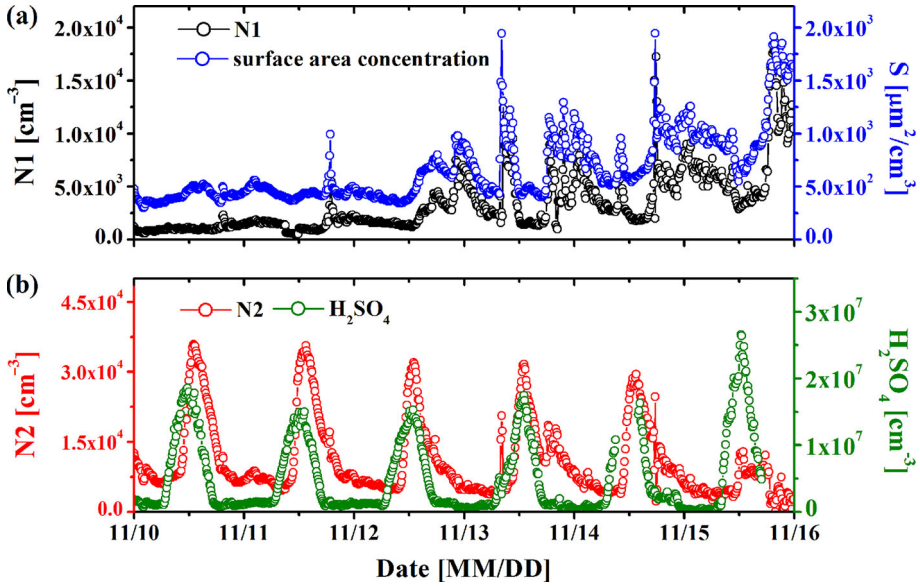

Fig. 7. Time series of (a) N1 (black) and particle surface area concentration (blue); (b) N2 (red) and sulphuric acid concentration during the episode (green).

Particle volume concentration increases at the rate of 6.1 $\mu m^3/cm^3$ per day during the episode. Organics and sulphates are the major contributors, accounting for 42 and 35% of the particle mass concentration, respectively. The contributions of primary species show significant elevation from 16% at 10–20 $\mu g/m^3$ to 30% at over 60 $\mu g/m^3$. The maximum ratio of primary emission to total mass concentration could reach 37% during the intensive biomass burning plume.

The contribution of accumulation mode particles to the total particle number concentration is close to 70% when the mass concentration caused by local emissions is more than 25 $\mu g/m^3$. A rough method is applied to quantify the contributions of different sources to the particle number concentration in this study. On average, the local biomass burning and secondary transformation provide 28 and 72% to particle number concentration and 21 and 79% to mass concentration, respectively.

5. Acknowledgments

This work was supported by the National Natural Science Foundation of China (21025728, 20977001, 21190052), and the China Ministry of Environmental Protection's Special Funds for Scientific Research on Public Welfare (201009002). We thank the 3C-Star 2008 team for their help.

References

Andreae, M. O., Schmid, O., Yang, H., Chand, D., Yu, J. Z. and co-authors. 2008. Optical properties and chemical composition of the atmospheric aerosol in urban Guangzhou, China. *Atmos. Environ.* **42**, 6335–6350.

Birmili, W. and Wiedensohler, A. 2000. New particle formation in the continental boundary layer: meteorological and gas phase parameter influence. *Geophys. Res. Lett.* **27**, 3325–3328.

Du, J., Cheng, T., Zhang, M., Chen, J., He, Q. and co-authors. 2012. Aerosol size spectra and particle formation events at Urban Shanghai in Eastern China. *Aerosol Air Qual. Res.* **12**(6), 1362–1372.

Dunn, M. J., Jimenez, J. L., Baumgardner, D., Castro, T., McMurry, P. H. and co-authors. 2004. Measurements of Mexico City nanoparticle size distributions: observations of new particle formation and growth. *Geophys. Res. Lett.* **31**, L10102.

Gong, Y. G., Hu, M., Cheng, Y., Su, H., Yue, D. and co-authors. 2010. Competition of coagulation sink and source rate: new particle formation in the Pearl River Delta of China. *Atmos. Environ.* **44**, 3278–3285.

Hagler, G. S. W., Bergin, M. H., Salmon, L. G., Yu, J. Z., Wan, E. C. H. and co-authors. 2006. Source areas and chemical composition of fine particulate matter in the Pearl River Delta region of China. *Atmos. Environ.* **40**, 3802–3815.

Hamed, A., Joutsensaari, J., Mikkonen, S., Sogacheva, L., Dal Maso, M. and co-authors. 2007. Nucleation and growth of new particles in Po Valley, Italy. *Atmos. Chem. Phys.* **7**, 355–376.

Hamed, A., Korhonen, H., Sihto, S.-L., Joutsensaari, J., Järvinen, H. and co-authors. 2011. The role of relative humidity in continental new particle formation. *J. Geophys. Res.* **116**, D03202.

Huang, X. F., He, L. Y., Hu, M., Canagaratna, M. R., Kroll, J. H. and co-authors. 2010. Characterization of submicron aerosols at a rural site in Pearl River Delta of China using an Aerodyne High-Resolution Aerosol Mass Spectrometer. *Atmos. Chem. Phys. Discuss.* **10**, 25841–25869.

Huang, X. F., He, L. Y., Hu, M., Canagaratna, M. R., Kroll, J. H. and co-authors. 2011. Characterization of submicron aerosols at a rural site in Pearl River Delta of China using an Aerodyne High-Resolution Aerosol Mass Spectrometer. *Atmos. Chem. Phys.* **11**, 1865–1877.

Jaatinen, A., Hamed, A., Joutsensaari, J., Mikkonen, S., Birmili, W. and co-authors. 2009. A comparison of new particle formation events in the boundary layer at three different sites in Europe. *Boreal. Environ. Res.* **14**, 481–498.

Kannosto, J., Virtanen, A., Lemmetty, M., Makela, J. M., Keskinen, J. and co-authors. 2008. Mode resolved density of atmospheric aerosol particles. *Atmos. Chem. Phys.* **8**, 5327–5337.

Kuang, C., McMurry, P. H., McCormick, A. V. and Eisele, F. L. 2008. Dependence of nucleation rates on sulfuric acid vapor concentration in diverse atmospheric locations. *J. Geophys. Res.* **113**, D10209.

Kulmala, M., Dal Maso, M., Makela, J. M., Pirjola, L., Vakeva, M. and co-authors. 2001. On the formation, growth and composition of nucleation mode particles. *Tellus B* **53**, 479–490.

Kulmala, M., Petaja, T., Monkkonen, P., Koponen, I. K., Dal Maso, M. and co-authors. 2005. On the growth of nucleation mode particles: source rates of condensable vapor in polluted and clean environments. *Atmos. Chem. Phys.* **5**, 409–416.

Kulmala, M., Vehkamaki, H., Petaja, T., Dal Maso, M., Lauri, A. and co-authors. 2004. Formation and growth rates of ultrafine atmospheric particles: a review of observations. *J. Aerosol. Sci.* **35**, 143–176.

Li, X., Duan, L., Wang, S., Duan, J., Guo, X. and co-authors. 2007. Emission characteristics of particulate matter from rural household biofuel combustion in China. *Energ. Fuel.* **21**, 845–851.

Lin, P., Hu, M., Wu, Z., Niu, Y. and Zhu, T. 2007. Marine aerosol size distributions in the springtime over China adjacent seas. *Atmos. Environ.* **41**, 6784–6796.

Liu, S., Hu, M., Wu, Z. J., Wehner, B., Wiedensohler, A. and co-authors. 2008. Aerosol number size distribution and new particle formation at a rural/coastal site in Pearl River Delta (PRD) of China. *Atmos. Environ.* **42**, 6275–6283.

Lohmann, U. and Feichter, J. 2005. Global indirect aerosol effects: a review. *Atmos. Chem. Phys.* **5**, 715–737.

Mikkonen, S., Romakkaniemi, S., Smith, J. N., Korhonen, H., Petäjä, T. and co-authors. 2011. A statistical proxy for sulphuric acid concentration. *Atmos. Chem. Phys.* **11**, 11319–11334.

Monkkonen, P., Koponen, I. K., Lehtinen, K. E. J., Hameri, K., Uma, R. and co-authors. 2005. Measurements in a highly

polluted Asian mega city: observations of aerosol number size distribution, modal parameters and nucleation events. *Atmos. Chem. Phys.* **5**, 57–66.

Poschl, U. 2005. Atmospheric aerosols: composition, transformation, climate and health effects. *Angew. Chem. Int. Ed.* **44**, 7520–7540.

Riipinen, I., Sihto, S. L., Kulmala, M., Arnold, F., Dal Maso, M. and co-authors. 2007. Connections between atmospheric sulphuric acid and new particle formation during QUEST III-IV campaigns in Heidelberg and Hyyti. *Atmos. Chem. Phys.* **7**, 1899–1914.

Rodriguez, S. and Cuevas, E. 2007. The contributions of ''minimum primary emissions'' and ''new particle formation enhancements'' to the particle number concentration in urban air. *J. Aerosol. Sci.* **38**, 1207–1219.

Rose, D., Wehner, B., Ketzel, M., Engler, C., Voigtlander, J. and co-authors. 2006. Atmospheric number size distributions of soot particles and estimation of emission factors. *Atmos. Chem. Phys.* **6**, 1021–1031.

Seinfeld, J. H. and Pandis, S. N. 1998. *Atmospheric Chemistry and Physics. From Air Pollution to Climate Change*. John Wiley, New York, pp. 429–443.

Sihto, S. L., Kulmala, M., Kerminen, V. M., Dal Maso, M., Petaja, T. and co-authors. 2006. Atmospheric sulphuric acid and aerosol formation: implications from atmospheric measurements for nucleation and early growth mechanisms. *Atmos. Chem. Phys.* **6**, 4079–4091.

Sioutas, C., Delfino, R. J. and Singh, M. 2005. Exposure assessment for atmospheric ultrafine particles (UFPs) and implications in epidemiologic research. *Environ. Health Perspect.* **113**, 947–955.

Stier, P., Seinfeld, J. H., Kinne, S. and Boucher, O. 2007. Aerosol absorption and radiative forcing. *Atmos. Chem. Phys.* **7**, 5237–5261.

Vakkari, V., Laakso, H., Kulmala, M., Laaksonen, A., Mabaso, D. and co-authors. 2011. New particle formation events in semi-clean South African savannah. *Atmos. Chem. Phys.* **11**, 3333–3346.

Wang, Z. B., Hu, M., Yue, D. L., Zheng, J., Zhang, R. Y. and co-authors. 2011. Evaluation on the role of sulfuric acid in the mechanisms of new particle formation for Beijing case. *Atmos. Chem. Phys.* **11**, 12663–12671.

Wu, Z. J., Hu, M., Lin, P., Liu, S., Wehner, B. and co-authors. 2008. Particle number size distribution in the urban atmosphere of Beijing, China. *Atmos. Environ.* **42**, 7967–7980.

Xiao, R., Takegawa, N., Zheng, M., Kondo, Y., Miyazaki, Y. and co-authors. 2011. Characterization and source apportionment of submicron aerosol with aerosol mass spectrometer during the PRIDE-PRD 2006 campaign. *Atmos. Chem. Phys.* **11**, 6911–6929.

Yli-Juuti, T., Riipinen, I., Aalto, P. P., Nieminen, T., Maenhaut, W. and co-authors. 2009. Characteristics of new particle formation events and cluster ions at K-puszta, Hungary. *Boreal. Environ. Res.* **14**, 683–698.

Yuan, B., Liu, Y., Shao, M., Lu, S. H. and Streets, D. G. 2010. Biomass burning contributions to ambient VOCs species at a receptor site in the Pearl River Delta (PRD). *China. Environ. Sci. Technol.* **44**, 4577–4582.

Yue, D. L., Hu, M., Wu, Z. J., Guo, S., Wen, M. T. and co-authors. 2010. Variation of particle number size distributions and chemical compositions at the urban and downwind regional sites in the Pearl River Delta during summertime pollution episodes. *Atmos. Chem. Phys.* **10**, 9431–9439.

Zheng, J., Hu, M., Zhang, R., Yue, D., Wang, Z. and co-authors. 2011. Measurements of gaseous H_2SO_4 by AP-ID-CIMS during CAREBeijing 2008 Campaign. *Atmos. Chem. Phys.* **11**, 7755–7765.